Construction and Building Materials 254 (2020) 119224

Contents lists available at ScienceDirect

Construction and Building Materials

journal homepage: www.elsevier.com/locate/conbuildmat

Prediction of cast-in-place concrete strength of the extradosed bridge deck based on temperature monitoring and numerical simulations

Aleksandra Kuryłowicz-Cudowska *, Krzysztof Wilde, Jacek Chróścielewski

Department of Mechanics of Materials and Structures, Faculty of Civil and Environmental Engineering, Gdańsk University of Technology, Narutowicza 11/12, 80-233 Gdańsk, Poland

HIGHLIGHTS

- Augmented maturity method using FEM-based numerical tests in addition to the usual laboratory and field experimental methodology.
- Recommendations for an effective laboratory research program and a reliable temperature measurement system.
- FEM analysis of compressive strength distribution in the concrete deck of extradosed bridge.
- The complex system of concrete monitoring improves the confidence of decisions on prestressing tendons or formwork removal and provides economic benefit.

ARTICLE INFO

Article history:
Received 19 April 2019
Received in revised form 10 April 2020
Accepted 15 April 2020

Keywords:
Cast-in-place concrete
Temperature of concrete
Early-age compressive strength
Augmented maturity method
Numerical simulations
Extradosed bridge

ABSTRACT

The work is devoted to the implementation of a monitoring system for high performance concrete embedded in the span of an extradosed bridge deck using a modified maturity method augmented by numerical simulations conducted by the authors' FEM code. The paper presents all research stages of bridge construction and considers the conclusions drawn from the results of laboratory tests, field measurements, and numerical calculations. The monitored structure is the largest extradosed bridge in Europe in terms of the span's length. Due to the considerable size and duration of the investment, it was beneficial to use an alternative method for estimating the compressive strength of concrete based on the maturity function. The bridge sections were investigated in three stages: in summer, autumn, and early spring (in June, September, and March). The monitoring of in-place concrete provided information on the actual temperature of the concrete and its gradients. Based on recorded temperatures and proposed numerical procedures, the actual strength of the cast-in-place concrete and the optimal dates of prestressing were determined. This contributed to shortening the work cycle and speeding up the work schedule.

1. Introduction

Currently, the development of technical infrastructure is largely based on cement and concrete composites. Research studies are focused on improving the parameters of building materials and strive to reduce construction costs. The primary motivation to analyse the assessment of concrete compressive strength on the basis of temperature was the interest of contractors of concrete structures in increasing the certainty, quality, and optimization of building works. Newly constructed bridges are primarily made of concrete. In addition, the number of structures built of prestressed concrete is increasing compared to those of reinforced concrete. In Poland, the ratio was 25.3–60.4% in 2007, respectively, and 41.0–44.2% in 2016. For prestressed structures, the time at which the concrete reaches the required compressive strength is the most important factor, not only for bridges but also for residential buildings. That allows for the start of the post-tension tendons. Because concrete works are being performed during extreme weather conditions, information on the cast-in-place concrete strength is crucial.

The thermal influences in young concrete are studied by many scientific teams [1–4]. The researchers consider maturity method for various types of concrete. Velay-Lizancos et al. [5] examined the influence of fine and coarse recycled aggregates on the accuracy of the maturity method. The authors found that a unique curve for vibrated and self-compacting concrete can be used independent of the percentage of recycled aggregate. Ji Jin et al. [6] investigated the prediction of the compressive strength of

* Corresponding author.
E-mail address: aleksandra.kurylowicz-cudowska@pg.edu.pl (A. Kuryłowicz-Cudowska).

https://doi.org/10.1016/j.conbuildmat.2020.119224
0950-0618/

early-age epoxy resin concrete and concluded that the maturity method is a non-destructive test useful for cast-in-place applications. Zhang et al. [7] presented a maturity concept supported by new experimental evidence for predicting the development of the mechanical properties of high-performance concrete over time.

In the early stages of the construction process, the monitoring of concrete hardening is a practical source of knowledge about the advancement of the cement hydration. The present study is focused on predicting the compressive strength of early age concrete, in real time. On the building site, temperature changes in the hardening concrete are relatively easy to measure. Currently, measuring the concrete temperature not only provides information about the occurrence of significant temperature gradients, but also enables the estimation of the in-place compressive strength of concrete. The measurement techniques allow the tracking of concrete temperature changes in the structure and transfer the obtained data to research teams. The usage of a wide range of additives, admixtures, aggregates [8–13], and various types of cement makes each concrete different, and thus the monitoring of the concrete structure becomes an individual task. The measurement module of concrete temperature can be also a part of the structural health monitoring system, e.g., [14,15].

In Poland, the assessment of concrete strength is carried out on samples taken from each batch of concrete, i.e., every 50 m^3 for bridge structures. During the construction of the subject bridge, approximately 330 batches of concrete were made, and 3300 concrete samples were collected and tested. This generates a lot of work including the necessity of recycling the large number of concrete specimens.

This paper proposes extensions and modifications of the applicable research procedures within the maturity method according to ASTM C1074 [16] and its development in the form of supplementation with a numerical program to determine the actual strength of concrete over time and volume of the monitored structure or structural segment. The authors' finite element method code was implemented in the construction process of the extradosed bridge built in Ostróda, in northern Poland. The application of the proposed technology made it possible to determine the post-tension dates for every segment of the bridge deck.

2. Augmented maturity method – procedure with numerical simulations

The cast-in-place compressive strength of concrete can be determined using two groups of methods. The first one, conventional and widely used, is expressed as the strength of standard specimens taken from mixtures delivered to the construction site. These samples are cured in laboratory conditions (at a temperature of 20 ± 2 °C and relative humidity ≥ 95% [17]) and tested at specified time intervals. The disadvantage of this approach is the required inference about the concrete strength of the structure based on the test results of samples curing under completely different conditions than the concrete in a real structure.

The second method, applied in the present research, states that the assessment of the mechanical properties of concrete can be done in real time based on thermal history and previously conducted laboratory tests [1,16]. The maturity method is founded on the assumption that for concrete hardening in variable temperature conditions, when the same level of maturity is reached, the concrete achieves the same strength. First, the strength-maturity relationship for a specific concrete should be determined. Next, the concrete temperature in the structure is measured from the moment when the mixture is placed in the formwork until the concrete reaches the desired strength. Using the maturity curve, developed in laboratory conditions, it is possible to estimate the actual concrete strength in the structure. The scheme of laboratory tests in regard to ASTM C1074 standard [16] is shown in Fig. 1.

The compressive strength results from 50-mm cubic samples stored in a water bath at three temperatures are the background to determine the datum temperature T_o and Q constant (activation energy divided by the gas constant, $Q = E_a/R$). This sample size ensures an identity between the mortar and ambient temperature, i.e., water bath. The selection of three temperatures depends on the concrete destination and weather conditions. The terms of mortar compression tests should be adjusted to the hydration rate. The obtained strength data allows the calculation of the rate constant for strength development k using linear regression (A.1.1.7 and A.1.1.8.2 of ASTM C1074 [16]) and non-linear regression according to Eqs. (1) and (2) [18]. The strength-age data should be approximated using the exponential function proposed by Freiesleben Hansen and Pedersen [2]:

$$S = S_u \cdot \exp\left(-(\tau/t)^{\beta}\right), \tag{1}$$

where S means compressive strength at time t, S_u is the ultimate compressive strength, τ is the time constant, and β is the shape constant, or using the Carino's hyperbolic equation [19]:

$$S = S_u \cdot \frac{k \cdot (t - t_0)}{1 + k \cdot (t - t_0)}. \tag{2}$$

In Eq. (2), the time t_0 represents the age at which the strength development begins, thus Eq. (2) does not consider the setting period.

ASTM C1074 standard [16] defines two maturity functions for the calculation of the maturity index based on the concrete

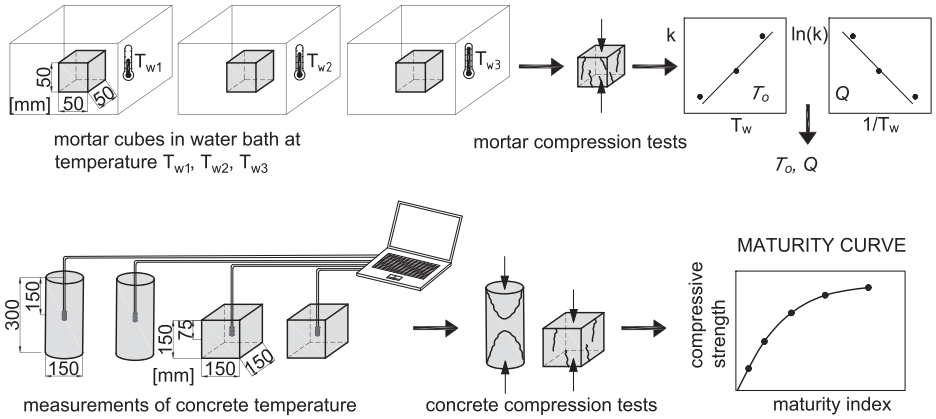

Fig. 1. Overview of the laboratory tests of maturity method.

temperature history. One of them, using an Arrhenius type law, is expressed by the equivalent age t_e of concrete:

$$t_e = \sum e^{-\frac{Q}{T}\left(\frac{1}{T}-\frac{1}{T_r}\right)}\Delta t, \quad (3)$$

where T_r means the reference temperature. In contrast to the temperature-time factor M, Eq. (3) uses a non-linear relationship between the initial strength rate and the curing temperature.

The next step is focused on compression tests of the concrete samples. The ASTM C1074 standard [16] suggests moulding 15 cylindrical samples: 2 are intended for temperature measurements and the others for destructive tests performed on 5 specified dates (1, 3, 7, 14, and 28 days). The procedures described above are the basic way to implement the maturity method in a construction site.

The proposed comprehensive method to estimate the concrete strength of a bridge deck considers modified assumptions of the maturity method and numerical calculations within the finite element method. The novel element of this paper is a complex solution for in-place concrete strength estimation, including laboratory, field, and numerical tests. The concept of the research algorithm is illustrated in Fig. 2. The suggested procedure has been applied during the construction of the extradosed bridge, and the conclusions gained from this work have been included in the proposed method.

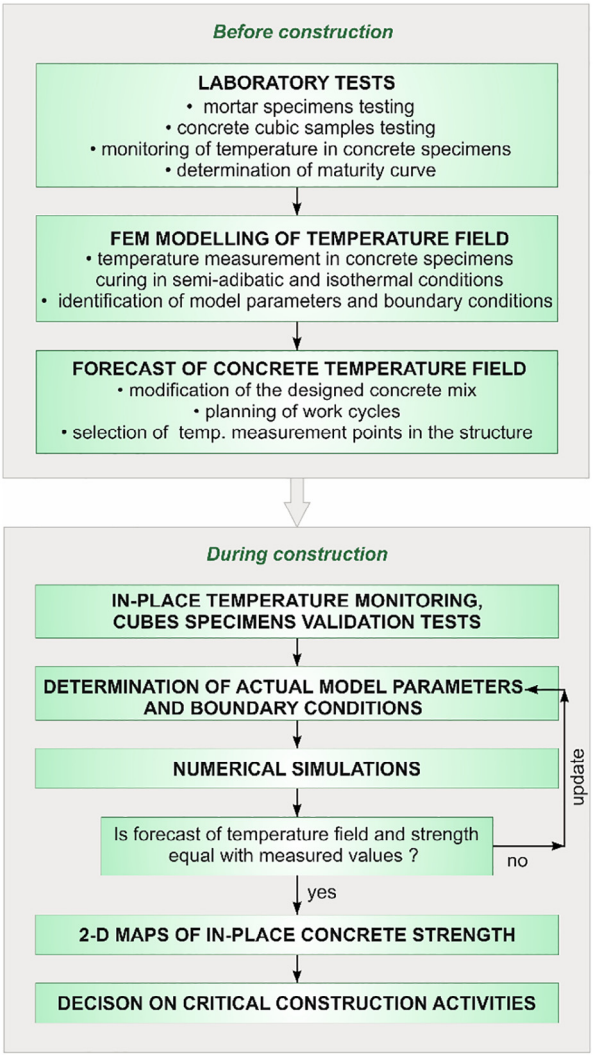

Fig. 2. The research algorithm.

The first remarks relate to the laboratory studies. To simplify the tests on mortar samples, compression tests should be performed in the constant time interval appropriate to the rate of strength increase. The determination of k-constants using the linear regression proposed in A1.1.7 and A.1.1.8.2 [16] is an incorrect solution, because the character of the strength gain at an early age is strongly nonlinear. After analysing linear and nonlinear procedures for the extradosed bridge data, it was determined that the best results are provided by the nonlinear regression of the strength-age data using the exponential function proposed by Freiesleben Hansen and Pedersen [2,20]. Due to the wide range of admixtures and additives used in the currently designed mixture, the determination of k and then the Q value by the empirical method is more advantageous than adopting the activation energy based on the literature data, in which the cement type is the only factor. In addition, k-constants computed on the basis of mortar samples combine the dependence not only on temperature but also on strength. Studies performed on mortar cubes allow the definition of the maturity function for a concrete under consideration. The conducted analysis indicated that calculations of the maturity index expressed in the form of the equivalent age t_e are more appropriate. In comparison to the temperature time factor M, the studies conducted by authors and the other researchers [21,22] have shown that Eq. (3) better describes the effect of higher concrete temperatures in the early age and largely eliminates discrepancies between the strength–maturity relationship for various early hardening temperatures.

ASTM C1074 [16] recommends drawing the maturity curve based on cylindrical samples, but also permits tests on concrete cubes. The conducted research indicates that the cubic specimens provide more repeatable results of compressive strength, and their availability on Polish construction sites is definitely larger. Due to the fact that concrete is a heterogeneous material and taking into account the authors' experience as well as European standards [23], the minimum number of cubic samples to be tested is equal to 17 (5·3 + 2), and the concrete compression test dates should be adapted to each case individually. It is also proposed to introduce additional data laboratory tests at the age of 56 days. The knowledge of the later-age strength of concrete (the ultimate strength) will increase the accuracy of the maturity curve approximation.

To describe the concrete strength–maturity relationship, suitable solutions are the hyperbolic curve proposed by Carino [19], the exponential curve of Freiesleben Hansen and Pedersen [2], as well as Chin's hyperbolic function [24]. Another function that properly describes the strength development of concrete versus the maturity index can also be used, for example, the power function applied in the case of the investigated high performance concrete. The comparison of mentioned functions is demonstrated in a paper [20]. The least suitable and not recommended is Plowman's logarithm equation [25]. Carino [1] noted that it does not provide proper results in terms of the low and high values of the maturity index (at early and late stages). Galobardes et al. [26] examined the maturity method for the application of sprayed concrete. The authors concluded that due to the influence of the accelerator in the hydration kinetics of cement, Plowman's formulation provides a poor correlation between the maturity index and the compressive strength. The above remarks constitute a set of our own and other authors' experiences that will be used to develop the best individual maturity curve for a specific concrete.

Due to the fact that the in situ concrete temperature measurements are limited to the selected few points, the most important aspect is getting to know the temperature distribution in the whole volume of the embedded concrete using Finite Element Method (FEM) modelling. In the next part of the paper, the thermo-chemical modelling and finite element procedure is described.

Our own method to identify model parameters, based on temperature registration in cubic samples curing in semi-adiabatic and isothermal conditions, has been adopted [27]. Considering boundary conditions, the convective heat transfer coefficients were determined experimentally with the use of atmospheric condition data. A forecast of the temperature field in concrete before starting construction provides the potential of using proper curing techniques or allows the eventual modification of the designed mixture. The complex approach including heat transport modelling and the improved maturity method favourably affects the prediction of the compressive strength distribution, which opens new possibilities of planning the working cycles, especially for the repeated sections of structure (e.g., sections of bridge span).

The presented work focuses on the real construction process of a large and relatively complex bridge structure that is dynamic and prone to unexpected changes. Thus, the integration and cooperation between the chief engineer and the scientific team working at the construction site and laboratory is very important and is the key factor to the success or failure of the proposed maturity method application.

2.1. Thermo-chemical aspect of concrete hydration

The process of concrete hardening is related to the change of phase composition of the medium [28]. A thermodynamic analysis allows for the determination of the amount of heat exchanged by the cement medium passing through one equilibrium state to another and for the control of the rate of those changes. As a result of heat conduction, a temperature field appears in every area of the concrete body. The energy balance in relation to the First Law of Thermodynamics may be stated:

$$\dot{E}_{in} + \dot{E}_g - \dot{E}_{out} = \dot{E}_{st}, \tag{4}$$

where E_{in} is the input energy, E_g is the energy generated due to cement hydration, E_{out} is the output energy, and E_{st} is the energy stored within the representative elementary volume [29]. The internal heat source associated with the hydration reaction causes a spatial temperature field variation. In the macroscopic approach, we can assume that concrete is an isotropic and homogeneous material, thus the thermal conductivity λ is spatially constant. Finally, the partial differential equation of a parabolic type is obtained:

$$\nabla \cdot (\lambda \nabla T) + q_c = \rho c \dot{T}. \tag{5}$$

The heat conduction Eq. (5) can be expressed as a function of the derivate of concrete temperature in regard to time $\dot{T}$, volumetric heat generation rate q_c, specific mass ρ, and specific heat of the material c.

Based on the fact that the model describes the temperature evolution from the moment the concrete is mixed, the initial condition can be expressed by the initial temperature of the concrete mixture, T_0. The energy balance equation between the concrete surface and the environment (air movement or insulation layer) can be expressed by Newton's (convection) [3] or Stefan-Boltzmann's (radiation) condition. The heat flux at the concrete surface must be absorbed by the surrounding air. Irrespective of the driving force for air movement, the heat flow from the element surface can be written using Newton's law:

$$q_0 = \alpha (T_{surf} - T_{env}), \tag{6}$$

where α is the heat transfer coefficient, and T_{env} and T_{surf} are the ambient and concrete surface temperatures, respectively.

The numerical simulation intended to supplement the maturity method should be based only on the temperature measurements at the few selected locations within the structure. The calculations must be as simple as possible because the numerical results must be available in real time, i.e., immediately on request by the construction manager. Therefore, the authors stated that a coupled model such as Di Luzio–Cusatis's [30] approach (thermo-chemo-hygro-mechanical model with two reactions expressed by the degree of hydration and the silica reaction) would be too complex for in situ applications. Finally, formulations developed by Cervera et al. [31] have been adopted. This model simplifies the heat transport equation by omitting the heat movement of migrating moisture, and it assumes that the heat transport is carried out only through conduction. According to many authors, the influence of moisture diffusion on heat transfer in concrete is not significant [32,33].

Cervera's model consists of two coupled equations: the thermal equilibrium (7) and the chemical kinetics equation expressed as a function of the evolution of the hydration degree (8):

$$\nabla \cdot \lambda \nabla T + Q_\xi \dot{\xi} = \rho c \dot{T}, \tag{7}$$

$$\dot{\xi} = \tilde{A}(\xi)\, exp\left(-\frac{E_a}{R\,T}\right). \tag{8}$$

The following parameters: ρ, c, λ, material constant Q_ξ (heat of cement hydration in concrete), activation energy E_a, and gas constant R, are responsible for the heat transfer phenomenon. In this model, a normalised internal variable, i.e., the hydration degree ξ that concerns the advancement of the hydration reaction, was introduced [34]. The rate of the internal heat source expressed in Eq. (5) is described by the formula: $q_c = Q_\xi \dot{\xi}$. Due to the thermally activated nature of cement hydration, a strong dependence ξ on temperature T is observed. The function of hydration progress $\tilde{A}(\xi)$ is expressed as the product of the chemical affinity and permeability, thus, the rate of hydration is finally expressed by the formula:

$$\dot{\xi} = \underbrace{\frac{\kappa}{n_0}\left(\frac{A_0}{\kappa}\frac{1}{\xi_{\max}} + \xi\right)(\xi_{\max} - \xi)\, exp\left(-\bar{n}\frac{\xi}{\xi_{\max}}\right)}_{\tilde{A}(\xi)=A^{-}\ \eta\ \text{(normalised chemical affinity)}} \underbrace{exp\left(-\frac{E_a}{R\,T}\right)}_{\text{(Arrhenius typ law)}} \tag{9}$$

Normalised chemical affinity $\tilde{A}(\xi)$ is directly measurable during an adiabatic calorimetric test. The three parameters κ/n_0, A_0/κ, and $\bar{n}$ are adjusted through a regression analysis by fitting the function $\tilde{A}(\xi)$ to the results of the calorimetric experiment [31].

2.2. Finite element procedure for nonlinear thermal problem

The adoption of the mathematical description of hardening concrete allows for relatively quick simulations of selected thermo-mechanical properties of the concrete, provided that the boundary conditions are correctly described. The structure of the proposed program for the numerical solution of the initial-boundary value problem by means of the Finite Element Method (FEM) is described below.

The heat balance is expressed by the transient Fourier equation for heat conduction with internal sources:

$$\nabla \cdot (\lambda \nabla T) + q_c - \rho c \dot{T} = 0 \; on \; structural \; body \; B \tag{10}$$

where ρ and c are constants, λ is the constitutive diagonal tensor containing λ_x, λ_y, and λ_z (constant), $q_c = Q_\xi \dot{\xi}$ means the internal rate of energy production by hydration, and $\nabla T = \frac{\partial T}{\partial x}\boldsymbol{e}_x + \frac{\partial T}{\partial y}\boldsymbol{e}_y + \frac{\partial T}{\partial z}\boldsymbol{e}_z$, (Fig. 3).

The boundary conditions of the analysed concrete structures may be limited only to Dirichlet:

$$T(x,y,z;\ t) = \bar{T}_{\partial B_T}(x,y,z;\ t) \; for \; t > 0 \; on \; \partial B_T \tag{11}$$

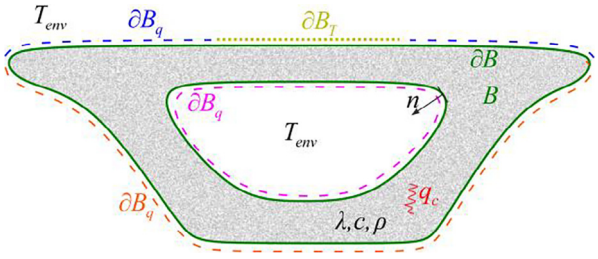

Fig. 3. The structural body.

and convective (Newman):

$$(-\lambda\nabla T)\cdot\boldsymbol{n} = \alpha(T - T_{env}) = q_0 \text{ for } t > 0 \text{ on } \partial B_q \tag{12}$$

boundary conditions, where $\bar{T}_{\partial B_T}$ is the prescribed temperature on boundary ∂B_T, T_{env} is the environmental temperature, α is the heat transfer coefficient, q_0 is the heat flux on boundary ∂B_q, $-\lambda\nabla T = \boldsymbol{q}$ is the heat flux, and $\boldsymbol{n}$ is the unit vector pointing out of the structural body (Fig. 3). In addition, it is assumed that the initial conditions are defined in the form:

$$T(x, y, z, t = 0) = T_0(x, y, z) \text{ on } B \tag{13}$$

In this study, a two dimensional Lagrange family n-node ($n = 4, 9, 16$) solid element is adopted. For the spatial discretization of the thermal problem, standard isoparametric finite elements are employed [35]:

$$x(\boldsymbol{\zeta}) = \mathbf{N}_{(e)}(\boldsymbol{\zeta})\mathbf{x}^e,\ y(\boldsymbol{\zeta}) = \mathbf{N}_{(e)}(\boldsymbol{\zeta})\mathbf{y}^e,\ T(\boldsymbol{\zeta}, t) = \mathbf{N}_{(e)}(\boldsymbol{\zeta})\ \mathbf{T}_{(e)}(t) \tag{14}$$

In the above equation, $\mathbf{N}$ denotes the interpolation matrix, $\boldsymbol{\zeta} = (\zeta^1, \zeta^2) \in [-1, +1] \times [-1, +1] \subset \mathbb{R}^2$ parent coordinates, $\mathbf{T}_{(e)}(t)$ designates the nodal temperatures, and $\mathbf{x}^e$, $\mathbf{y}^e$ are the nodal coordinates for a given finite element with volume $B_{(e)}$ and edge $\partial B_{(e)}$. The weak form for the thermal equations (accounting for the Newman and trivially fulfilling the Dirichlet conditions) becomes:

$$\int_{B_{(e)}} \nabla\mathbf{N}_{(e)}^T\lambda\nabla T dB - \int_{B_{(e)}} \mathbf{N}_{(e)}^T Q_\xi\dot{\xi} dB + \int_{B_{(e)}} \mathbf{N}_{(e)}^T\rho c\dot{T} dB + \int_{\partial B_q\cap\partial B_{(e)}} \mathbf{N}_{(e)}^T\alpha T_{(e)} d(\partial B) - \int_{\partial B_q\cap\partial B_{(e)}} \mathbf{N}_{(e)}^T\alpha T_{env} d(\partial B) = \mathbf{0} \tag{15}$$

After spatial discretization, the resulting finite element equations on $B_{(e)} \cup \partial B_{(e)} \Rightarrow B \cup \partial B$ are:

$$\mathbf{M}_{(e)}\dot{\mathbf{T}}_{(e)} + \left[\mathbf{K}_{M(e)} + \mathbf{K}_{L(e)}\right]\mathbf{T}_{(e)} = \mathbf{f}_{q_c(e)} + \mathbf{f}_{T_{env}(e)} \Rightarrow \mathbf{M}\dot{\mathbf{T}}(t) + \mathbf{K}\mathbf{T}(t) = \mathbf{f}(t) \tag{16}$$

$$\mathbf{K}_{M(e)} = \int_{B_{(e)}} \nabla\mathbf{N}_{(e)}^T\lambda\nabla\mathbf{N}_{(e)} dB, \mathbf{K}_{L(e)} = \int_{\partial B_q\cap\partial B_{(e)}} \mathbf{N}_{(e)}^T\alpha\mathbf{N}_{(e)} d(\partial B), \tag{17}$$

$$\mathbf{M}_{(e)} = \int_{B_{(e)}} \mathbf{N}(e) T\rho c\mathbf{N}_{(e)} dB, \tag{18}$$

$$\mathbf{f}_{q_c(e)} = \int_{B_{(e)}} \mathbf{N}_{(e)}^T q_c dB = \int_{B_{(e)}} \mathbf{N}_{(e)}^T Q_\xi\dot{\xi} dB, \mathbf{f}_{T_{env}(e)} = \int_{\partial B_q\cap\partial B_{(e)}} \alpha T_{env}\mathbf{N}_{(e)}^T d(\partial B) \tag{19}$$

where $\mathbf{K} = A_{e=1}^{n_{(e)}}\left[\mathbf{K}_{M(e)} + \mathbf{K}_{L(e)}\right]$ is the conductivity matrix, $\mathbf{M} = A_{e=1}^{n_{(e)}}\mathbf{M}_{(e)}$ is the capacity matrix, $\mathbf{f} = \mathbf{f}_{q_c} + \mathbf{f}_{T_{env}} = A_{e=1}^{n_{(e)}}\left\{\mathbf{f}_{q_{c(e)}}\right\} + A_{e=1}^{n_{(e)}}\left\{\mathbf{f}_{T_{env(e)}}\right\}$ equals the load vector, n_e is the number of finite elements, and $A_{e=1}^{n_{(e)}}$ is the standard assembling operator. This equilibrium equation is ready for the time approximation.

For the transient response, Eq. (16) should be integrated with respect to time. Thermal problems with nonlinearities, due to the dependency of the hydration rate on the temperature, expressed in an Arrhenius-type law (9) and variable boundary conditions, require incrementally-iterative techniques. In this study, the backward-Euler integration scheme for t_{n+1} (20) in two-level iterative procedure is adapted (at a structural level for $\mathbf{T}_{n+1}^{(I)}$ (21) and at a local level for $\xi_{n+1}^{(i)}$ (22)). The solution of the concrete temperature field as a function of time consists of the following approximation:

$$\dot{T}_{n+1} = \frac{T_{n+1} - T_n}{\Delta t},\ \ \dot{\xi}_{n+1} = \frac{\xi_{n+1} - \xi_n}{\Delta t}, \tag{20}$$

$$\left(\frac{1}{\Delta t}\mathbf{M} + \mathbf{K}\right)\mathbf{T}_{n+1}^{(I)} = \mathbf{f}_{n+1}^{(I)} + \frac{1}{\Delta t}\mathbf{M}\mathbf{T}_n,\ \mathbf{f}_{n+1}^{(I)} = \mathbf{f}_{T_{env}\ n+1} + \mathbf{f}_{q_c\ n+1}^{(I)} \tag{21}$$

$$\frac{1}{\Delta t}\left(\xi_{n+1}^{(i)} - \xi_n\right) - \frac{k}{n_0}\cdot\left(\frac{A_0}{k\cdot\xi_\infty} + \xi_{n+1}^{(i)}\right)\cdot\left(\xi_\infty - \xi_{n+1}^{(i)}\right) \cdot e^{\left(-n^{-\frac{\xi_{n+1}^{(i)}}{\xi_\infty}}\right)}\cdot e^{\left(-\frac{E_a}{R\cdot T_{n+1}^{(I)}}\right)} = 0. \tag{22}$$

where $\Delta t = t_{n+1} - t_n$ is the time-step.

The implementation of the Newton-Raphson method allows for the solution of Eq. (22) and the extraction of the hydration degree $\xi_{n+1}^{(i)}$ related to the local temperature $T_{n+1}^{(I)}$, which is achieved using a standard interpolation over the nodal concrete temperatures $\mathbf{T}_{n+1}^{(I)}$. This nodal temperature $\mathbf{T}_{n+1}^{(I)}$ is assured by an 'outer' Newton-Raphson algorithm stated at the structural level by Eq. (21). The hydration rate $\dot{\xi}_{n+1}^{(i)}$ is calculated from Eq. (22) $\dot{\xi}_{n+1}^{(i)} = \frac{1}{\Delta t}(\xi_{n+1}^{(i)} - \xi_n)$ after solving Eq. (22) for $\xi_{n+1}^{(i)}$. Eq. (20), according to Eq. (19) $\mathbf{f}_{q_c(e)\ n+1}^{(I)} = \int_{B_{(e)}} \mathbf{N}_{(e)}^T Q_\xi\dot{\xi}_{n+1}^{(i)} dB$ supplies a new trial vector for $\mathbf{f}_{q_c\ n+1}^{(I)}$, and as a result improves the solution for $\mathbf{T}_{n+1}^{(I)}$ by Eq. (21), [31]. The time-step using the numerical integration of the hydration degree should be lower than the one assumed for the structural problem, because the hydration rate $\dot{\xi}$ is mostly greater than $\dot{T}$. An interpolation is needed to determine the sub-incremental values of the temperature at the integration point within time-steps (Eq. (22)), [31]. In this paper, a linear interpolation between T_n and $T_{n+1}^{(I)}$ was adopted.

3. The extradosed bridge located in Ostróda

The considered structure is a 4-span road bridge (Fig. 4). The total length of the deck equals 677.0 m (2 × 132.5 m + 2 × 206.0 m). The structure was built using a cantilever-forming traveller. The main spans are 206 m long, and they are divided into 52 segments. This bridge is one of the largest extradosed bridges in the world and the longest extradosed structure in Europe in terms of the span length. The superstructure of the bridge is typical and has the form of a three-chambered box with a total width of 28.4 m (Fig. 5) made of high performance concrete, C 60/75 class. The deck height changes from 4 m in the spans to 6 m in the support zones.

A volume of 34809 m^3 of concrete was used for the construction of the bridge, including 1275 m^3 of non-structural concrete class C 12/15–C 20/25 and 33534 m^3 of structure concrete C 25/30–C 60/75, and 19646 m^3 of C 60/75 concrete was used for the construction of a span. The construction process lasted from June

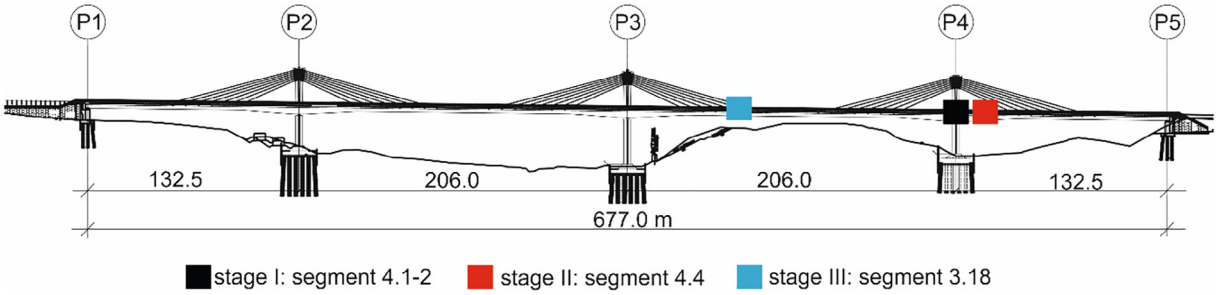

Fig. 4. View of the bridge with monitored zones.

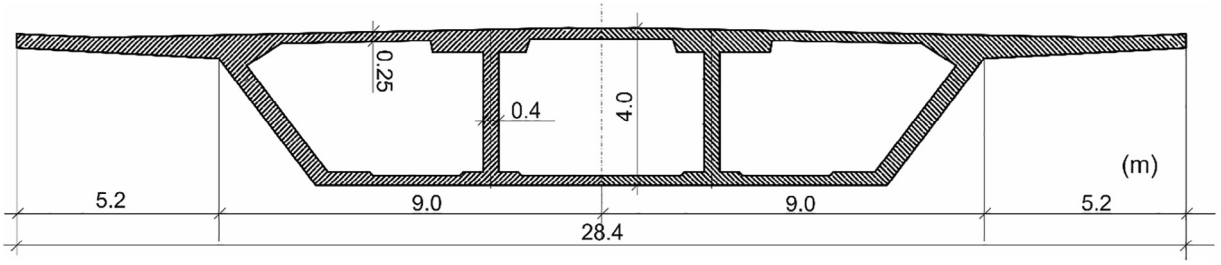

Fig. 5. Cross section number 3.18.

2015 to December 2017, when the bridge passed the loading tests [36].

The technological project of the bridge construction divided the deck into assembly sections:

nos. 1–2 – start sections over the support, 15.2 m long, variable height;
nos. 3–6 – overhanging sections, 3.6 m long, variable height;
nos. 7–10 – overhanging sections, 4.0 m long, variable height;
nos. 11–26 – overhanging sections, 4.0 m long, fixed height;
closer segment – 2 m long.

The monitoring of the concrete hardening was implemented for three sections (4.1–2, 4.4, and 3.18) built in a different way. The concreting of the starting section (no. 4.1–2) located above the P4 support was divided into four stages: the bottom plate, webs and support transverse beam, the top plate between the outer webs, and the top plate – the external cantilever of the plate. The value of 60% of the characteristic strength of the built-in concrete constituted the minimum value for prestressing the structure in the following order: transverse post-tension of the top plate, transverse post-tension of the bottom plate, and longitudinal post-tension of the starting section. For the case of the overhanging section no. 4.4, casting operations included two stages: the bottom plate and webs and then the top plate. For the span section, not hung, with a fixed construction height (no. 3.18), concreting with the entire cross-section was carried out.

The formwork of the bridge deck consisted of 3-SO plywood and H20N beams spaced at approximately 30 cm. For the overhanging segments, the shuttering on the outer circuit was insulated with Styrofoam FS-15, 10 cm thick.

The original project approach was to prestress each section of the deck after 3 days of concrete placement. To shorten this time, the contractor together with technologists imposed the design of C 60/75 high performance concrete to be able to prestress the structure after 48 h. The compressive strength of the designed concrete was supposed to rise by 1 MPa/h.

4. Implementation of research procedures at the bridge construction site

4.1. Laboratory tests

Laboratory tests were carried out on three sets of 50-mm mortar cubes (a total of 54 specimens), 20 cylindrical (150/300 mm), and 26 cubic (150 mm) samples made of concrete according to the recipe given in Table 1. The scope of research included compression tests on mortar and concrete specimens and temperature measurements inside concrete samples. Cement (Table 2), fine and coarse aggregate as well as additives and admixtures from the concrete plant indicated by the contractor were taken. The details of the considered mortar and concrete samples are described in the authors' previous work [20].

4.1.1. Mortar tests

The mortar cubes (18 per set) were cured in a water bath at the temperatures: $T_{w1} = 5\,^{\circ}C$, $T_{w2} = 24\,^{\circ}C$, $T_{w3} = 35\,^{\circ}C$. Compression tests for cubes stored at 24 and 35 °C were carried out after 1, 2, 3, 5, 7, and 14 days, but the tests were conducted on samples cured at 5 °C after 2, 3, 4, 5, 7, and 14 days due to the lower rate of strength gain in low temperatures. The strength-age relationships shown in the Fig. 6 were calculated using the exponential Eq. (1), discussed in Section 2, and fit by a least-squares regression to the data.

Table 1
Overview of mix proportions.

Component	(kg/m^3)
CEM I 52.5N SR3/NA	440
Water	143
Sand 0/2	632
Basalts 2/8	498
Basalts 8/16	785
Plasticisers	8.49

Table 2
Chemical and physical properties of cement.

Component	CEM I 52.5N SR3/NA
SO_3	2.6%
Cl-	0.07%
Na_2O	0.5%
Al_2O_3	3.9%
C_3A	1.8%
$C_3AF + 2C_3A$	18.9%
SiO_2	20.8%
CaO	66.2%
C_3S	59.9%
C_2S	16.4%
Density	3.2 g/cm^3
Specific surface area	3789 cm^2/g
LOI	1.1%

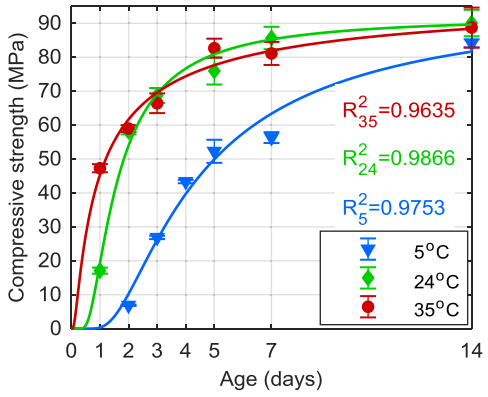

Fig. 6. The average compressive strength of mortar cubes: measured data and exponential regression Eq. (1).

The rapid hydration of mortar samples curing at 35 °C is incomparably higher than that at 5 °C, accepted as the minimum value for concrete cast in place (Fig. 6). After two days, the samples cured at 5 °C reached an average strength of 6.89 MPa. On the other hand, after 24 h, the cubes matured at 35 °C achieved 47.28 MPa. After 14 days, the highest strength was reached by the specimens stored at 24 °C (close to standard temperature), slightly lower for those stored at 35 °C, and the lowest for those stored at 5 °C, reaching 90.07, 88.73, and 84.07 MPa, respectively.

The constants T_o and Q were identified based on the relationship between the rate constants k for strength development and the curing temperature with use of linear and nonlinear regression procedures. The obtained values are summarised in Table 3. The results of the exponential regression were established to be meaningful because the strength estimated by the equivalent age and the measured strength were the most similar to each other. The hydration process slows down rapidly for the datum temperature equal to −1.0 °C. Considering the activation energy divided by the gas constant (4620 K), the maturity function of the considered high performance concrete expressed in the form of an equivalent age is determined to be:

$$t_e = \sum e^{-4620\left(\frac{1}{T} - \frac{1}{273.15+24}\right)}\Delta t. \quad (23)$$

4.1.2. Concrete tests

Cubic specimens ($8 \cdot 3 = 24$ cubes) were moulded at a concrete plant and then transported to the university laboratory where two samples of each type for measuring the concrete temperature were formed. Compression tests at 1, 2, 3, 5, 7, 14, 21, and 28 days were performed. The compliance criteria according to PN–EN 206-1 [23] (criterion I: $f_{cm} \geqslant f_{ck} + 4$ and criterion II: $f_{ci} \geqslant f_{ck} - 4$) were met. After 24 h, the tested concrete samples reached 40% of the 28-day strength.

The temperature evolution of the concrete specimens during the first four days (96 h) is shown in Fig. 7a. The initial temperature for the concrete was considered to be 22.9 °C. As a result of the exothermic hydration process, the maximum concrete temperature occurred in the 19th hour, and the average maximum temperature was equal to 29.2 °C.

The thermal history of the concrete samples, compressive strength results, and Eq. (23) are a complete data set for the development of the maturity curve of the concrete C 60/75 class. The proposed power function adequately fits the data as shown by the R^2 value (Fig. 7b). The other maturity-strength relationships described in Section 2 were also considered [20]. The most appropriate curve, suitable in the entire range, i.e., for low and high values of equivalent age t_e, was the power equation indicated in Fig. 7b.

4.1.3. FEM model

The implementation of numerical methods enable one-, two-, and three-dimensional models of the heat conduction equation to be solved [37]. In this work, the calculations of the hardening concrete in the bridge deck using a two-dimensional (2D) model were made. Forecasting the concrete temperature development allowed an estimation of the concrete strength in time, space, and volume of the tested bridge segment.

Numerical simulations of the concrete's temperature field were conducted using the authors' FEM code called MAI_Temp. Geometric parameters for the monitored overhanging section of the bridge were adopted from technical documentation. The c and λ values of concrete in agreement with the specific heat and thermal conduc-

Table 3
Regression analysis [20].

Regression type	T (°C)	(k1/day)	T_o (°C)	$R_{To}{}^2$ (–)	Q (K)	$R_Q{}^2$ (–)
Linear A.1.1.7 ASTM C1074	5	0.334	−1.3	0,9792	4766	0.9984
	24	1.052				
	35	1.750				
Linear A.1.1.8.2 ASTM C1074	5	0.162	−0.1	0,9961	5452	0.9863
	24	0.676				
	35	1.050				
Hyperbolic, Eq. (2)	5	0.254	−1.6	0,9711	4606	0.9998
	24	0.747				
	35	1.272				
Expotential, Eq. (1)	5	0.273	−1.0	0,9431	4620	0.9981
	24	0.749				
	35	1.397				

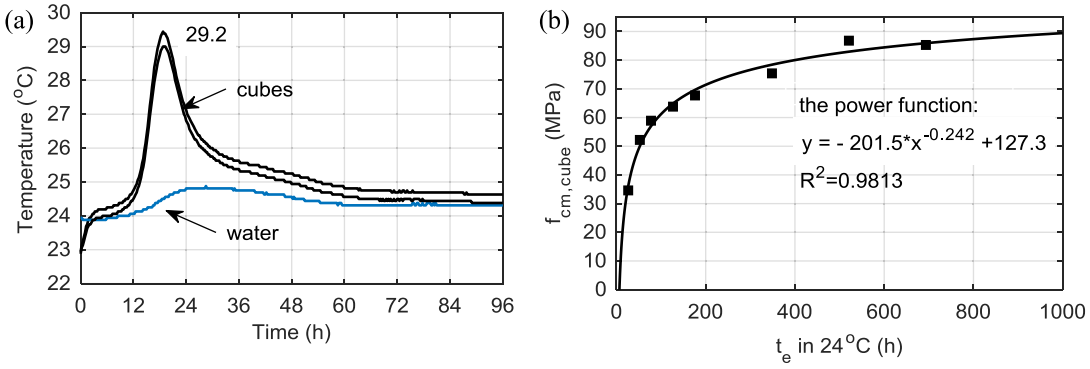

Fig. 7. (a) Temperature evolution of cubic specimens, (b) maturity curve related to cubic strength.

tivity of individual components were calculated according to the formulas proposed by Breugel and Lura [38]. The maximum heat of hydration Q_{max} was determined based on data from the cement producer. According to the Mills formula [39], the final hydration degree ξ_{max} was computed using the water-cement ratio.

To identify the parameters κ/n_0, $\bar{n}$, A_0/κ an adiabatic hydration curve was necessary. Therefore, a novel way to determine the above model parameters was proposed. First, temperature measurements in the concrete cubic samples curing in semi-adiabatic and isothermal conditions were performed. The next step was to formulate relationships for the three mentioned parameters, which strongly depend on atmospheric and geometry conditions. Due to the symmetry of the analysed cross-section, the calculations were made for half the cross-section. In the symmetry axis, the convective heat transfer coefficient $\alpha = 0$ was assumed. The boundary conditions indicated by green, red, and black contour lines were adopted in accordance with Fig. 8. The heat transfer coefficients α_{fc} for the free surface and α_s^{form} for the surface protected by the formwork were assumed. The average ambient temperature measured during the 10 days $\left(T_{env}^{10days}\right)$ was taken.

A mesh with nine-node quadrilateral surface elements and three-node linear elements on the edges was used for space discretization of the section. In terms of the formal use of the finite element method, a convergence analysis of the solution was carried out. The FEM model was generated using 7370 surface finite elements, 1380 linear finite elements, and 30,860 nodes. The GID program was used to generate a mesh of the cross-section and then to postprocess and produce a graphical presentation of the results.

4.2. Monitored sections

Due to the different concrete technologies (start segments on stationary scaffolds, typical segments built up using cantilever technology), to the changing cross-section of the bridge box, and to various weather conditions (seasons), the bridge deck was monitored in three stages. The first stage included the monitoring of the start sections no. 4.1–2, executed in June. The second stage concerned the overhang section no. 4.4 with variable height (September), and the last stage was the overhang section no. 3.18 with a fixed height (March). The localization of the measurement segments is shown in Fig. 4. In Figs. 9–11, the monitored section zones are presented.

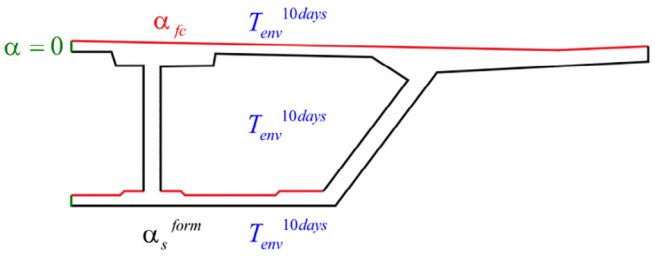

Fig. 8. Boundary conditions.

4.3. Novel measurement system

The new temperature measurement system designed and built for the field tests is shown in Fig. 12. The device makes it possible to measure the concrete temperature at 20 points simultaneously and works on water-resistant, digital 1-wire sensors, ds18b20 type. The temperature sensors can be assembled individually or by using a prefabricated strip with a series of detectors arranged in accordance with a pre-prepared project. This allows the minimization of wiring that is exposed to damage during construction works. The device can be powered with a battery for approxi-

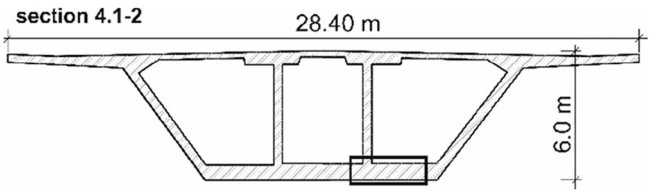

Fig. 9. Monitored section no. 4.1–2.

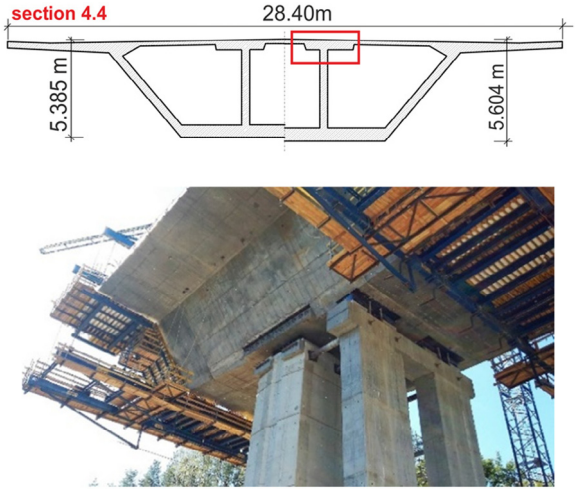

Fig. 10. Monitored section no. 4.4.

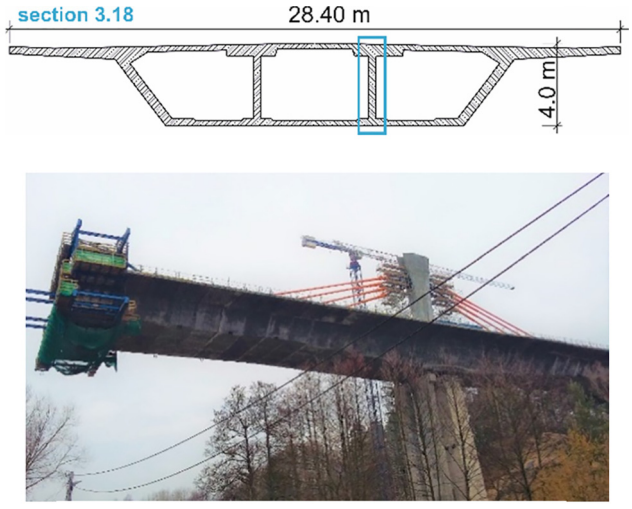

Fig. 11. Monitored section no. 3.18.

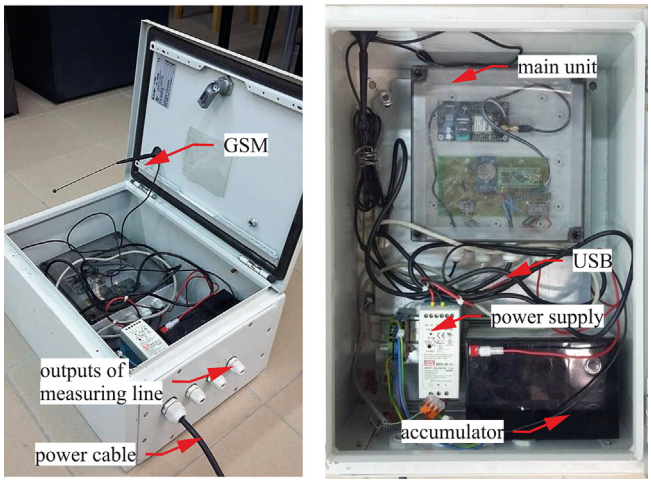

Fig. 12. Temperature measurement system.

mately 30 days, and the data is saved every 15 min by 20 sensors. This provides a total of 2880 values sent to the server every hour by a GSM modem. The ds18b20 sensors are specified to operate in a temperature range from −55 to 125 °C with an accuracy of ±0.5 °C and, what is important, does not require calibration. This guarantees the reliability of the measurement, in contrast to commonly used thermocouples whose disadvantage is the mechanical instability of the measuring connector and the possibility of electricity flowing outside the thermocouple when the joint is not insulated. The device has three diodes indicating its operation and information about the connected mains supply, data transmission, and GSM modem activity.

4.4. In situ measurements

4.4.1. Concrete temperature – Stage I

The first stage of the research focused on the bottom plate of the starting segment, located just above the support P4 (Figs. 4 and 9) [40]. The concrete temperature sensors were located in two cross-sections (A-A and B-B) of the bottom plate (points p1–p6) and in two cubes and cylinders (p7–p10). The ambient temperature above and below the plate (points o1, o2) and in the water bath (o3) was also monitored. The locations of the temperature sensors are given in Fig. 13.

Fig. 14 illustrates the registered thermal history at all measurement locations. Next to the coloured points, there is a depth indicted. This depth is measured from the upper surface of the plate. A "time zero" was assumed when the last of the sensors indicated a temperature of 26.7 °C (the initial temperature of the mixture).

The concrete works took place in June, with significant insolation, when the ambient temperature during the day reached 37 °C. The 14-day average ambient temperature was 21.5 °C, and the average wind speed was 4.44 m/s [41]. Such conditions favoured the increase in concrete temperature of the bottom plate, and hence the intensification of strength gains in the first days of hardening.

The maximum concrete temperature of the bottom plate was noted 25 h after concrete placing and reached a temperature of

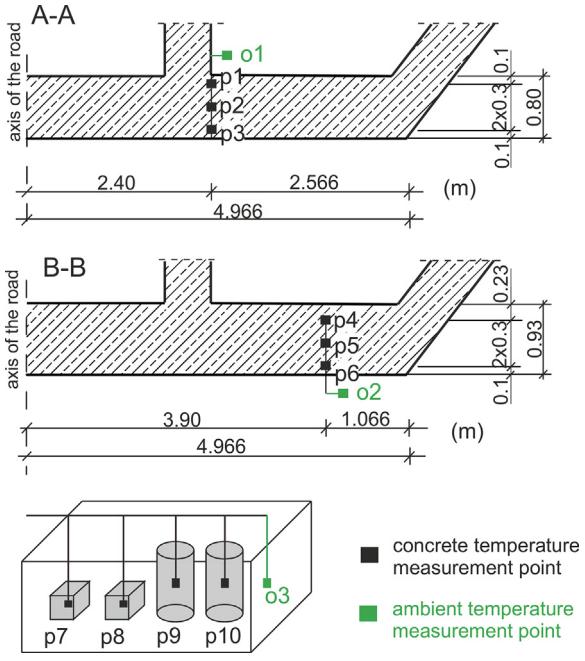

Fig. 13. Locations of temperature measurement points – section 4.1–2.

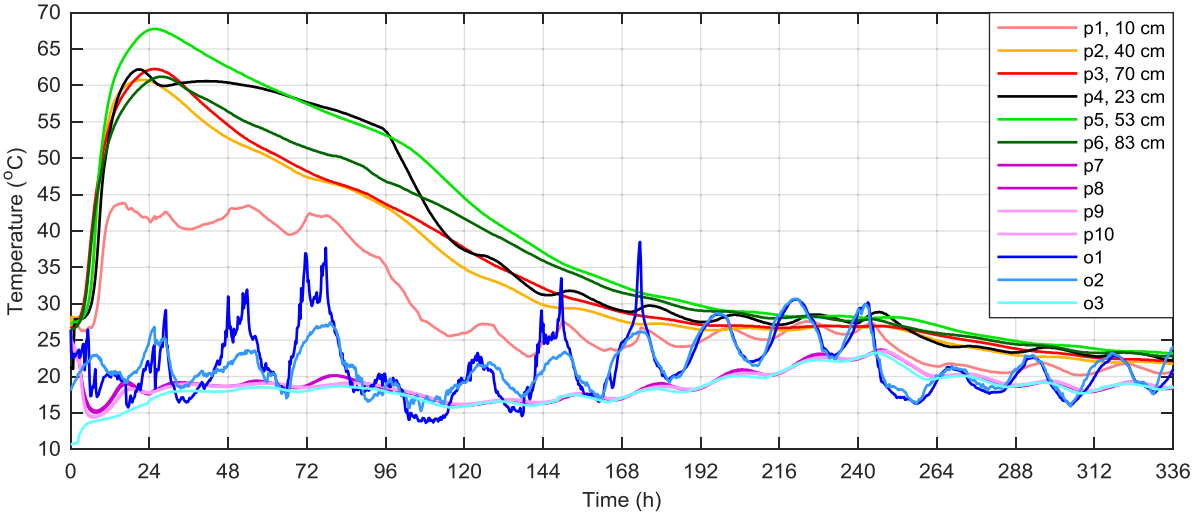

Fig. 14. Temperature evolution of concrete slab for 14 days.

67.8 °C at point p5. The temperature of 70 °C, which the standard PN–EN 13670 [42] indicates as the limit value, was not exceeded. The monitored element, 0.93 m thick, is called a massive element, inside which the conditions are close to adiabatic. The self-heating temperature of the concrete caused by cement hydration was 41.1 °C. After 25 h, a gradual decrease in the concrete temperature was observed. The largest temperature differences were recorded between the points located in the centre and near the top surface of the plate. For the A-A cross-section (0.80 m), at 24 h, the temperature difference between points p1 and p2, distant by 30 cm, was 19.3 °C. Such information induced the contractor to insulate the free surface of the slab, which was covered with a 5-cm-thick Styrofoam layer (from 25 to 94 h). This is clearly visible in the thermal history of points p1 and p4 located in the upper zone of the plate. Between 24 and 94 h, a constant concrete temperature was maintained.

The influence of the boundary conditions is mainly observed at the bottom and at the surface of the slab. In the lower part, there is formwork insulation (21-mm-thick plywood and wooden girders), and from the top, the plate is exposed to sunlight. The daily temperature fluctuations of the concrete are most visible from the 6th day of hardening at points located at the top surface of the slab, and the temperature stabilization of the concrete is observed after 10 days of hardening.

4.4.2. Concrete temperature – Stage II

The concreting of segment 4.4 (Fig. 10) was carried out with the balanced cantilever method using a movable scaffolding system (MSS). This section was built in two stages: first the bottom plate and webs, and a day later the top plate. The 10-day average ambient temperature was 20.1 °C, and the average wind speed was equal to 2.22 m/s [41].

In situ monitoring included temperature registration in the top slab (points p8–p14) near the tendon channels and in the internal web of the box girder (points p1–p7; Fig. 15). The measurements were carried out with dedicated prefabricated modules consisting of 9 sensors (7 for concrete and 2 for air temperature measurements). During the construction works, the p7 and p8 sensors were damaged, which was caused by an unexpected bending of cables near the formwork.

The concrete temperatures recorded in the top plate are depicted in Fig. 16. The initial temperature of the mix that was used for concreting the web was 29.1 °C, and in the case of the top plate, it was equal to 28.5 °C. The maximum concrete temperature for both monitored elements was noted after 17.5 h and reached the values of 57.8 and 59.6 °C, at point p4 and p12, respectively. Thus, the maximum temperatures of the self-heating caused by the cement hydration heat registered in the web and the top plate were 28.7 and 31.1 °C.

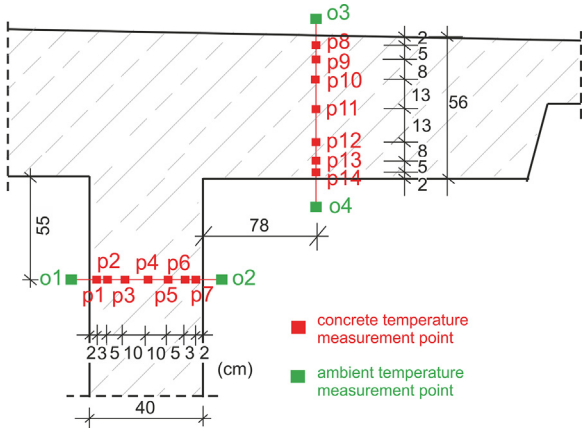

Fig. 15. Locations of temperature measurement points – section 4.4.

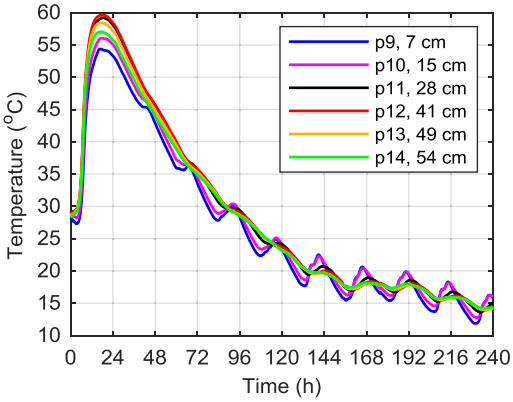

Fig. 16. Temperature development of the concrete inside the top slab for 240 h (10 days).

The temperature recorded in the web, surrounded on both sides with formwork, is very similar at all measurement points. The top plate is free on the one side and protected with shuttering on the other, which is a reason for the temperature difference (e.g., $\Delta p9 - p12 = 5.2$ °C). Due to the relatively high ambient temperature, these differences are not significant.

4.4.3. Concrete temperature – Stage III

The third stage of work was performed on section 3.18 (Fig. 4). The entire segment was concreted in one cycle. The 10-day average ambient temperature was 4.4 °C, and the average wind speed was 3.61 m/s [41].

The measurement cross-section was located in the middle of section 3.18, which had a thickness of 4 m. The temperature sensors were placed in the top slab (p1–p5), web (p6–p8), and bottom plate (p9–p13). The temperature registration in the deck was carried out with a prefabricated measuring module, which consisted of 13 sensors and was designed for this task. The temperature in the samples (p14, p15) and the air temperature over (o16), inside (o17, o18), and under the bridge box (o19) were also monitored (Fig. 17).

The monitored elements with thicknesses of 0.35, 0.40, and 0.57 m are so-called medium-sized concrete elements. The initial temperature of the concrete mix delivered to the construction site was 14.8 °C. The recorded temperature changes at all measurement points and in individual structural elements are illustrated in Figs. 18 and 19.

The concrete temperature of the bottom plate (Fig. 19a) is almost the same at all points. The maximum concrete temperature was equal to 34.7 °C (point p11) and occurred after 20 h.

In the web, the maximum recorded temperature (Fig. 19b) was 34.3 °C, which is approximately 23.5 °C lower than the maximum temperature registered for the same element during the second stage of research.

The temperature evolution in the top plate is the most diverse (Fig. 19c). The maximum concrete temperature was equal to 42.8 °C (at point p4), which was 16.8 °C lower than the maximum temperature recorded for the same element during the second stage of the research. The self-heating temperature caused by the cement hydration recorded in the top plate was 28.0 °C. Fig. 20 shows the temperature changes in the cross-sectional concrete measurements at 12, 24, 36, 48, 96, and 168 h. Different boundary conditions (formwork at the bottom, free top surface) and a low ambient temperature generated a temperature difference equal to 15.7 °C between the concrete core (p4) and the surface (p1) of the top plate. In general, the temperature difference should not be greater than 15–20 °C, depending on the thickness of the element.

The boundary conditions have the greatest influence on the intensity of the heat released during cement hydration (except for the mixture composition). The evolution of the concrete temperature depends strictly on the ambient temperature, geometry, formwork, and influence of adjacent concrete blocks. The homogeneous boundary conditions for the bottom plate or web cause the

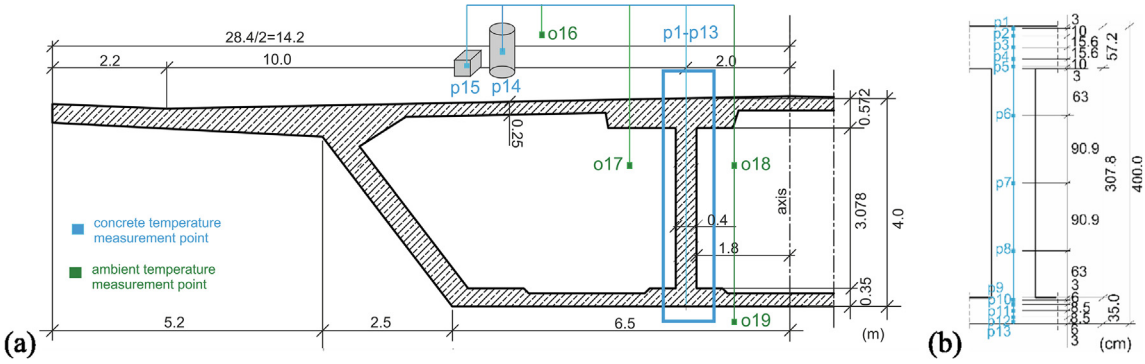

Fig. 17. Locations of temperature measurement points – section 3.18.

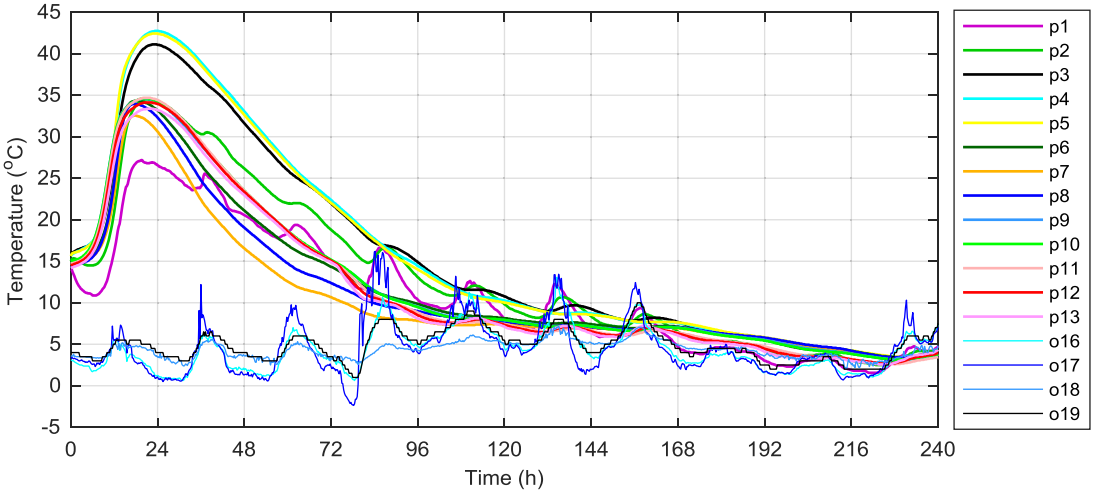

Fig. 18. Temperature evolution for 10 days.

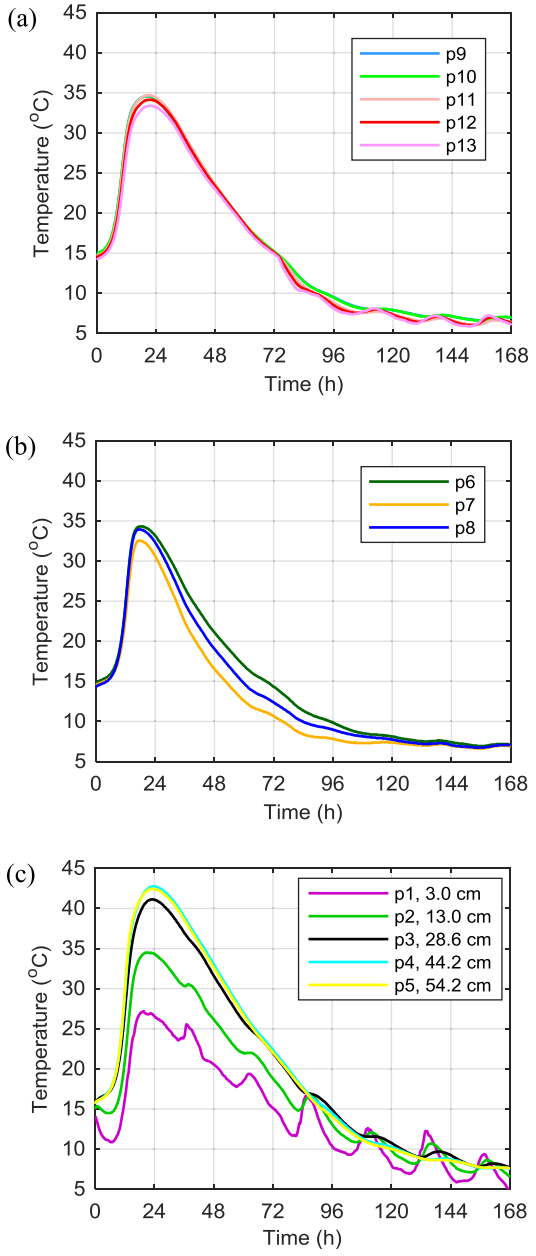

Fig. 19. Temperature development of the concrete for 168 h (7 days) inside: (a) the bottom slab, (b) the web, (c) the top slab.

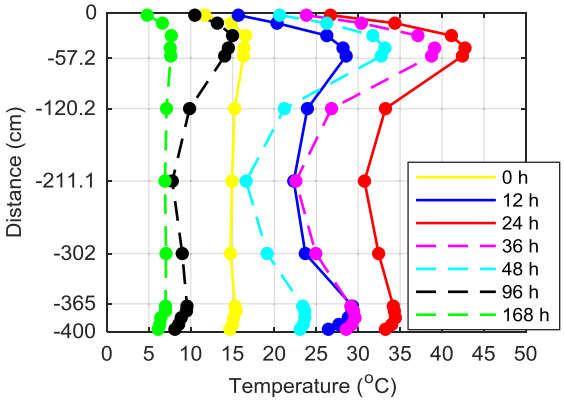

Fig. 20. The evolution of concrete temperature.

same temperature increase during the heating phase at all measurement points. For the top plate, the exposed top surface is subjected to additional daily temperature variations, causing significant gradients inside the hardening plate. Therefore, protecting the free surfaces of concrete elements is very important. The observations made in this paragraph are also valid for all the evaluated span sections.

4.4.4. Validation samples

The 150 mm cubic specimens moulded during the casting operations of each section of the bridge deck were used for validation studies. The continuous monitoring of the temperature in the concrete samples allowed the computation of the maturity index (in the form of equivalent age t_e), and with respect to the laboratory-tested compressive strength, the maturity-strength plot was updated. Three specimens were tested each time.

This approach enabled a real check of the concrete maturity curve developed during the initial phase. Destructive tests are also a good way to verify the concrete delivered to the construction site. The rate of compressive strength gain of the cubic specimens investigated during the first stage of the study was visibly higher than during the initial tests and also stage numbers two and three. This was probably due to different curing conditions (high ambient temperatures in June) or the fact that it was the first section, and technological conditions in the concrete plant varied in relation to the next segments. Therefore, the results of the compression tests of the cubic samples taken during the first stage of the research were rejected. Fig. 21 presents the final, updated maturity curve for concrete C 60/75 class.

5. Results – Compressive strength

5.1. Compressive strength at the selected locations

The measured temperature of the concrete sections as well as the developed maturity curves made it possible to plot the strength – age relationship for the selected points. In the third stage of the study, the visible strength increase during the first approximately 24 h is observed (Fig. 22). This is related to the amount of heat released, which in the initial phase is characterised by a significant intensity, and as the process continues, the cooling phase takes place, and the temperature of the hardening concrete stabilises.

At the age of 12 h, the concrete in the top plate reaches the cubic compressive strength of 11.1 MPa (acc. to p1), for the web 16.4 MPa (acc. to p7), and for the bottom plate 17.9 MPa (acc. to p13; Fig. 22). Thus, the highest early-age strength was noted in the bottom slab, and the lowest in the top one. The post-tension of the bridge span could have started after the concrete reached

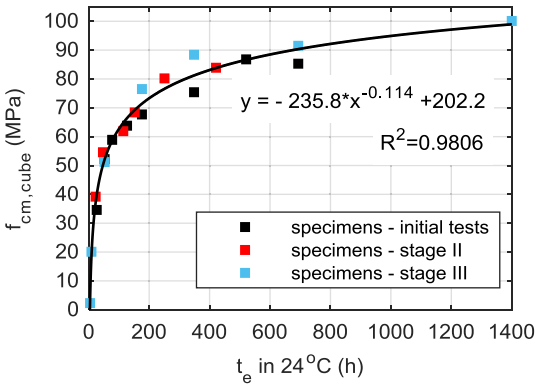

Fig. 21. Maturity curve related to cubic strength.

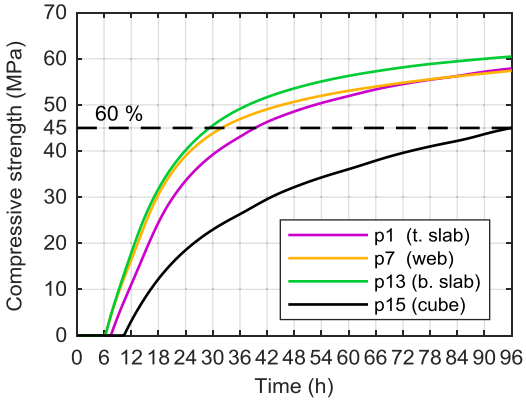

Fig. 22. Cubic strength of the section 3.18 (selected points: p1, p7, p13) and cubic sample (p15) versus age.

60% of the characteristic strength (45 MPa for class C 60/75). This level is reached for the concrete in the top plate (p1) in 39.3 h, for the web (p7) in 32.0 h, and for the bottom plate (p13) in 29.3 h. In turn, the 45 MPa strength, estimated on the basis of in-place temperature measurements in a cubic sample (p15), would be reached only after 4 days (95.9 h). The compressive strength determined during the destructive tests of the cubic samples, cured for first 24 h in building site and after that under standard conditions, was 51.2 MPa (68%) at the age of 48 h. The results from both cases proved that the assessment of in-place concrete based on specimens is inefficient and predicts an extended time to achieve required strength. After 28 days, the predicted strength of the top plate concrete is 79.3 MPa (acc. to p1), of the web 79.1 MPa (acc. to p7), and the bottom plate 79.6 MPa (acc. to p13). The strength requirements for class C 60/75 are met.

To compare the concrete strength gain in the three stages of the study, Fig. 23 summarises the strength development achieved during the individual stages and in the construction elements (b.s. - bottom slab, t.s. – top slab, web). This figure also shows air temperature changes. Representative strength curves were developed on the basis of the measurement points, for which the lowest concrete temperature was recorded (stage I according to p1, stage II according to p1 and p9, and stage III according to p1, p7, and p13). There is a significant difference in the concrete strength evolution in the structure at every stage, which proves how large the influence of

Table 4
60% of the characteristic strength.

60%·75 = 45 MPa/rate of strength gain		Time (h)	Rate (MPa/h)
Stage I	b.s.	13.7	3.3
Stage II	t.s.	15.1	3.0
	web	14.3	3.1
Stage III	t.s.	39.3	1.1
	web	32.0	1.4
	b.s.	29.3	1.5

the boundary conditions is, including air temperature, on the self-heating of concrete and thus on the compressive strength value (Fig. 23).

In Table 4, the time needed to achieve the level of 60% of the characteristic strength and the rate of strength increase are listed. In stage III, in relation to stages I and II, the estimated time is about twice as long. For stages I and II it is an average of 14.4 h, and for stage III, 33.5 h. Nevertheless, the rate of strength gain is significant and consistent with the project. In all cases, the technologist's assumption of regarding strength gain equal to 1 MPa/h, even at the temperature considered as minimum for concreting (5 °C), was met. In conclusion, the fastest possible date for the post-tension of the bridge section was set at 1.0–2.0 days, mainly dependent on atmospheric conditions.

5.2. FEM results

Based on the developed FEM program, maps of the concrete temperature and compressive strength distribution for the overhanging section (no. 3.18) were prepared. The thermophysical parameters of C 60/75 concrete were adopted in accordance with Table 5 and Table 6 using nomograms developed in paper [27].

Fig. 24 presents the concrete compressive strength calculated on the basis of concrete temperature measured during the third stage of the study and the maturity curve according to Fig. 21 (solid lines), as well as the strength obtained as a result of numerical calculations (dashed lines) for selected measurement points. The model shows similar strength evolutions as measured experimentally for the overhanging section of the bridge. It should be added that in the FEM model, a constant ambient temperature of 4.4 °C was adopted, and in the real structure, a significant effect from

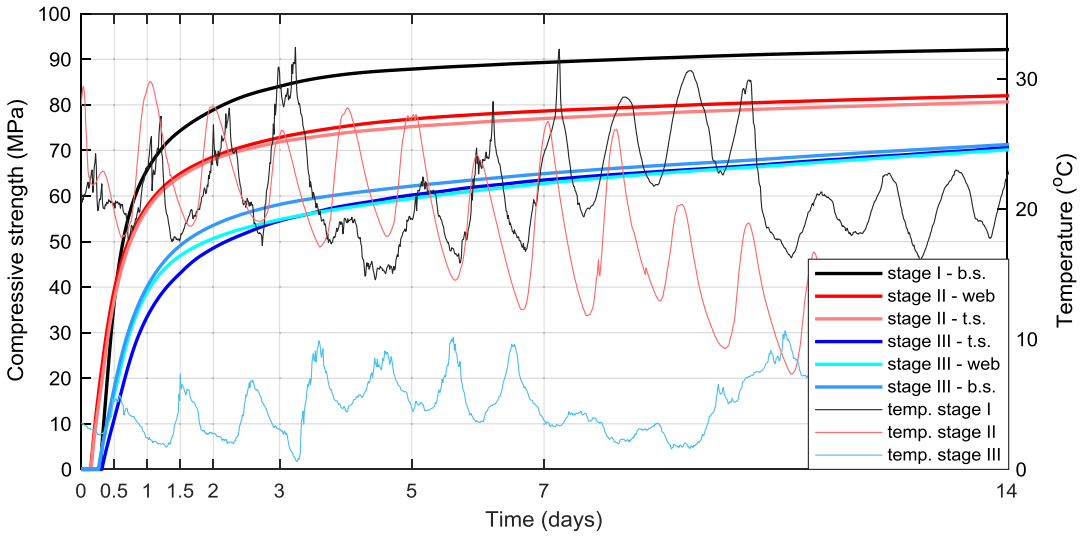

Fig. 23. Cubic compressive strength of structure in three stages and appropriate ambient temperature versus age.

Table 5
Thermophysical properties of concrete C 60/75 class.

C (kg/m^3)	ρ (kg/m^3)	E_a/R (K)	w/c (–)	ξ_{max} (–)	Q_{max} (kJ/kg)	c (kJ/(kg·K))	λ (W/(m·K))
440	2570	4620	0.325	0.65	330	0.84	2.0

Table 6
Model parameters – stage III.

κ/n_0 (1/h)	$\bar{n}$ (–)	A_0/κ (–)	T_0 (°C)	T_{env}^{10days} (°C)	α_s^{form} (W/(m^2·K))	α_{fc} (W/(m^2·K))
$12.0{\cdot}10^6$	4.0	$1{\cdot}10^{-4}$	14.8	4.4	5.6	10.3

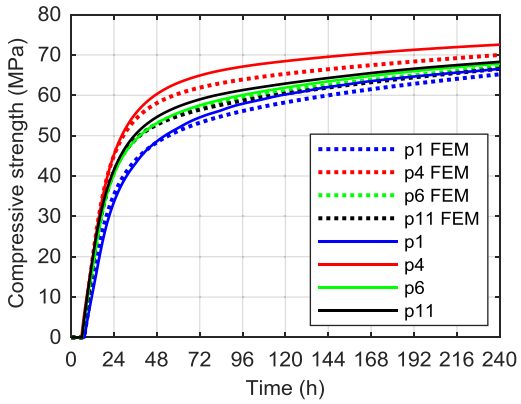

Fig. 24. The estimated compressive strength based on the measured temperature and temperature achieved from the numerical model at selected points of the analysed section.

the daily fluctuations of air temperature on the in-place concrete temperature is observed.

The maps of the concrete temperature field were made in a two-dimensional model. Table 7 reports the temperature maps of the concrete section in 12, 24, 48, 84, 240, and 672 h. After 24 h, for the top plate in the cross-section passing through the centre of the inner web, the temperature difference between the concrete surface of the bridge box (23.3 °C) and 40 cm below (40.8 °C) is equal to 17.5 °C (Table 7). The biggest source of thermal energy is located in places with the largest volume of embedded concrete. The internal and external web, due to the presence of formwork on both sides, is in the most uniform thermal state. The parts of the top and bottom slabs with the smallest thickness and the end of the plate cantilever are particularly susceptible to the cooling process. At the age of approximately 10 days, the cooling phase of the concrete ends, and throughout the entire section, a temperature close to the air temperature is observed (Table 7).

The results of the concrete temperature field in the bridge box allowed for elaborate maps of the concrete compressive strength

Table 7
FEM results.

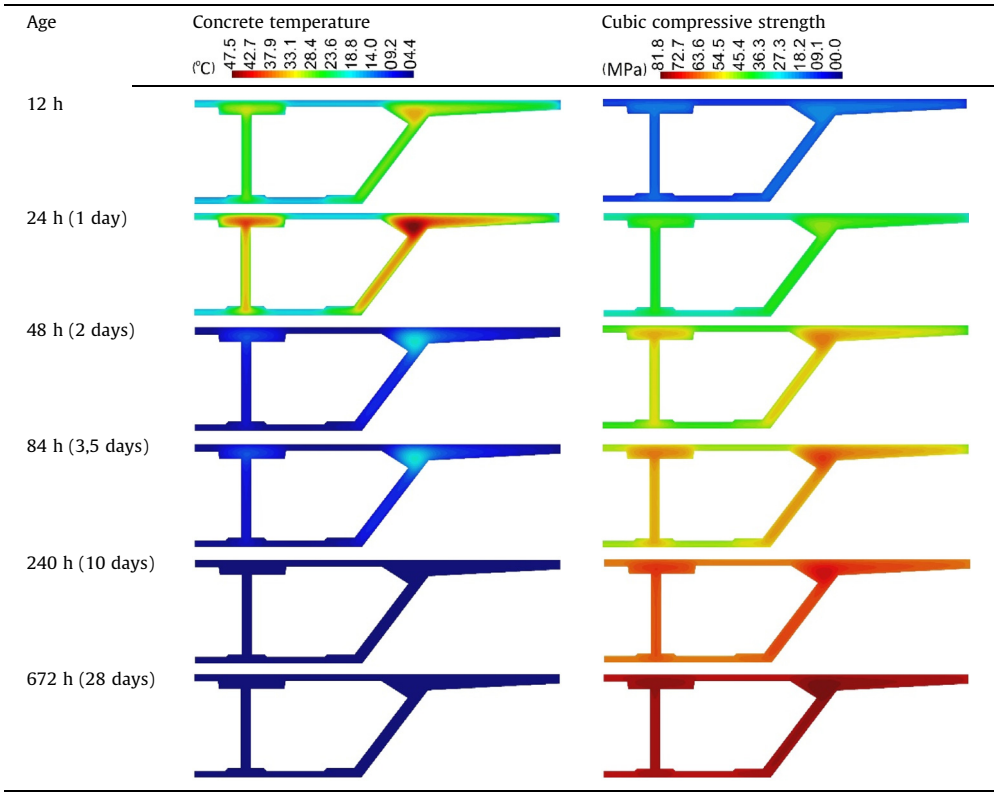

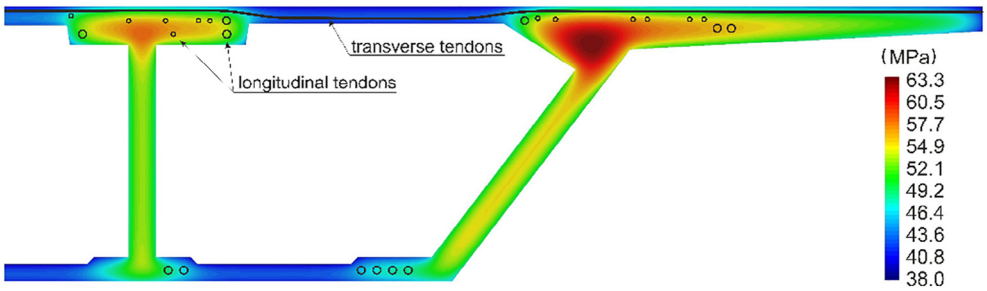

Fig. 25. Map of the cubic compressive strength of the overhanging section at the age of 48 h with indication of the position of tendons.

distribution (Table 7). At the age of 12 h, the strength of young concrete changes from 7.8 MPa for the free surface of the plates to 21.0 MPa for the zone with the largest amount of built-in concrete. At the age of 24 h, the minimum concrete strength equals 25.7 MPa and applies mainly to the corners and external zones of the 25-cm-thick top/bottom slab (Table 7).

At the age of 48 h, the compressive strength of concrete varies from 38.0 to 63.3 MPa. At point 5.1, the suggested possible date for starting the post-tension of the span section was determined to be 2 days, which is confirmed by FEM simulations for the cross-section passing through the centre of the inner box's web. However, the concrete in the thinnest part of the top and bottom slab, at the age of 48 h, does not reach the level of 60% of characteristic strength. The compressive strength of concrete equal to 45 MPa is achieved in the considered cross-section after 3.5 days of concrete placement (Table 7).

At the age of 28 days, high-performance concrete achieves a compressive strength of 75 MPa in the entire volume, thus meeting the requirements of class C 60/75 (Table 7).

A detailed analysis of the compressive strength variation at the age of 48 h is presented in Fig. 25. The picture also shows the location of the prestressing cable channels. The results allow the analysis of the concrete maturity in the neighbourhood of the plastic ducts to facilitate the decisions on speeding up the post-tensioning tendons. In the case of an unfavourable strength distribution in the vicinity of the prestressing channel, longer maturing periods might be chosen to ensure the safety of the conducted works.

The results of the numerical simulations emphasise the importance of the selection of the measurement points to estimate the concrete strength in the structure. The application of the maturity method extended by numerical calculations based on the FEM significantly increases the accuracy of the prediction method of the concrete strength in the structure. Before the concrete placement and the implementation of the monitoring system on the construction site, it is possible to conduct many numerical calculations to consider the different thermophysical parameters of the concrete and the initial-boundary conditions, e.g., the evaluation of the impact of Styrofoam insulation.

The application of these 2D calculations enables the accurate tracking of temperature and concrete strength changes in the entire cross-section of the concrete element. Such knowledge can be complementary material for the engineer and building inspector in the interest of the construction control process as well as to increase the work safety for the benefit of the final product quality.

6. Final remarks

The paper presents modified experimental and numerical procedures for estimating the early-age compressive strength of concrete using in-situ temperature measurements. The standard maturity method was analysed in a multithreaded way with regard to increasing its effectiveness. The results of laboratory tests showed some limitations and shortcomings of the method and provided ideas for its improvement. Based on the gained experiences from laboratory tests the following recommendations can be made:

- use the Freiesleben Hansen and Pedersen function to describe the strength-age data of mortar cubes and apply a nonlinear regression to determine the *k*-constants;
- express concrete maturity as a function of an equivalent age;
- approximate the maturity-strength data of high-performance concrete with the proposed power function and improve the approximation by adding a laboratory test at the age of 56 days;
- use only cubic specimens for maturity curve determination for practical reasons and to increase the certainty of the compressive strength results.

A very important practical aspect is the method of temperature measurement at the construction site. The following conclusions are drawn after the application of the authors' measurement system:

- to ensure the reliability of measurement, it is suggested to use digital 1-wire sensors, ds18b20 type, because they work on only one cable and do not require calibration;
- it is proposed to use prefabricated measurement rods on which the sensors are fixed to protect against accidental damage;
- the data acquisition system must have an independent power supply, resistant housing and the ability to send data through a wireless connection for online monitoring.

The analysis of the temperature and strength data obtained during all stages of measurements on the bridge deck allowed the formulation of the following findings:

- the parameter that significantly delays or accelerates the development of the temperature in the concrete deck is the ambient temperature and initial temperature of the concrete mix;
- temperature measurements in the concrete structure enables the proper care of individual sections e.g., to apply a Styrofoam layer;
- the destructive tests of the validation samples successfully verifies the maturity curve developed in the preparatory phase, which contributes to increasing the accuracy of the applied method;
- the concrete embedded in the bridge deck achieves the level of 60% of the characteristic strength required to prestress much faster (24–48 h after the concrete was placed) than it did in the evaluation carried out on the basis of the compression tests

of standard concrete sample, and this significantly accelerates the work schedule.

The authors' FEM code for modelling the temperature field in concrete and the detailed validation of the numerical model with respect to data collected in field studies was carried out. The main issues and advantages of the proposed two-dimensional FEM model are listed below:

- the 2D numerical calculations enable the prediction of the distribution of concrete compressive strength, the identification of places particularly exposed to slowing down the rate of strength gain and the detailed analysis of the strength distribution near the cable channels;
- the procedure of using tests of concrete hardening under isothermal and semi-adiabatic conditions allows for the proper definition of boundary conditions and model parameters;
- the biggest advantage of strength estimation based on the 2D model in comparison with the measurements in a limited number of points is the knowledge of local changes in strength in all areas of the entire analysed cross-section of the same structure;
- numerical results give the basis for the best selection of temperature measurement points in real structures.

The algorithm of the proposed augmented maturity method might be an important part of the design process of the mixture and construction of concrete structural elements. Knowledge of the maturity-strength relationship determined in laboratory conditions provides information on the development of concrete strength before the final concreting of the structure. The concrete monitoring system verifies the mixture delivered to the construction site and makes it possible to correct planned actions or adjust the parameters of the fresh mix. The proposed method also allows a limitation on the number of compression tests to monitor the condition of concrete in the structure. 2D maps of the sectional concrete strength of the extradosed bridge provided practically online during the construction improve the confidence at decision making stages and finally, due to benefits resulting from adjustments of the construction schedule, give an economic profit. The proposed algorithm of the augmented maturity method, with the developed package of the numerical solutions for predicting the development of temperature and strength of concrete, may be applied to any engineering structure with a complex geometry. An attempt to extend the predicted mechanical properties of concrete (tensile strength and Young's modulus) has already been undertaken; hence, the proposed method will be constantly developed and will consider that the FEM simulations must be fast because the results need to be available online almost simultaneously with the temperature measurements.

CRediT authorship contribution statement

Aleksandra Kuryłowicz-Cudowska: Conceptualization, Methodology, Software, Validation, Investigation, Data curation, Writing - original draft, Visualization, Project administration. **Krzysztof Wilde:** Conceptualization, Resources, Writing - review & editing, Supervision. **Jacek Chróścielewski:** Methodology, Software, Formal analysis, Supervision.

Declaration of Competing Interest

The authors declare that they have no known competing financial interests or personal relationships that could have appeared to influence the work reported in this paper.

References

[1] N.J. Carino, H.S. Lew, The maturity method: from theory to application, Proceedings of the Structures Congress & Exposition, May 21–23, Washington, D.C., American Society of Civil Engineers, Reston, Virginia, 2001.
[2] P. Freiesleben Hansen, E.J. Pedersen, Curing of Concrete Structures. Draft DEB – Guide to Durable Concrete Structures. Appendix 1, Comite Euro-International du Beton, Switzerland, 1985.
[3] J.E. Jonasson, P. Groth, H. Hedlund, Modelling of temperature and moisture field in concrete to study early age movements as a basis for stress analysis, in: International Symposium Thermal Cracking in Concrete at Early Ages, Munich, 1994, pp. 45–52.
[4] B. Klemczak, K. Flaga, A. Knoppik-Wrobel, Analytical model for evaluation of thermal-shrinkage strains and stresses in RC wall-on-slab structures, Arch. Civ. Mech. Eng. 17 (1) (2017) 75–95.
[5] M. Velay-Lizancos, I. Martinez-Lage, P. Vazquez-Burgo, The effect of recycled aggregates on the accuracy of the maturity method on vibrated and self-compacting concretes, Arch. Civ. Mech. Eng. 19 (2019) 311–321.
[6] N. Ji Jin, I. Seung, Y.S. Choi, J. Yeon, Prediction of early-age compressive strength of epoxy resin concrete using the maturity method, Constr. Build. Mater. 152 (2017) 990–998.
[7] J. Zhang, D. Cusson, P. Monteiro, J. Harvey, New perspectives on maturity method and approach for high performance concrete applications, Cem. Concr. Res. 38 (12) (2008) 1438–1446.
[8] E. Horszczaruk, P. Sikora, K. Cendrowski, E. Mijowska, The effect of elevated temperature on the properties of cement mortars containing nanosilica and heavyweight aggregates, Constr. Build. Mater. 137 (2017) 420–431.
[9] M. Kurpinska, B. Grzyl, A. Kristowski, Cost analysis of prefabricated elements of the ordinary and lightweight concrete walls in residential construction, Materials 12 (21) (2019) 3629.
[10] M. Kurpinska, L. Kułak, Predicting performance of lightweight concrete with granulated expanded glass and ash aggregate by means of using artificial neural networks, Materials 12 (12) (2019) 2002.
[11] A. Mariak, L. Grabarczyk, B. Wojtasik, M. Zbawicka, Influence of selected additives and admixtures on underwater concrete and the environment, MATEC Web Conf. 219 (2018) 03013.
[12] A. Mariak, M. Kurpińska, The effect of macro polymer fibres length and content on the fibre reinforced concrete, MATEC Web Conf. 219 (2018) 03004.
[13] E. Haustein, A. Kuryłowicz-Cudowska, The effect of fly ash microspheres on the pore structure of concrete, Minerals 10 (1) (2020) 58.
[14] M. Miśkiewicz, Ł. Pyrzowski, K. Wilde, Structural health monitoring system for suspension footbridge, in: Proceedings 2016 Baltic Geodetic Congress (Geomatics), IEEE, 2017, pp. 321–325.
[15] A. Mariak, M. Miśkiewicz, B. Meronk, Ł. Pyrzowski, K. Wilde, Reference FEM model for SHM system of cable-stayed bridge in Rzeszów, Adv. Mech.: Theor. Comput. Interdiscip. Issues (2016) 383–387.
[16] ASTM C1074, Standard Practice for Estimating Concrete Strength by the Maturity Method, ASTM, West Conshohocken, PA, 2019.
[17] EN 12390-2, Testing Hardened Concrete – Part 2: Making and curing Specimens for Strength Tests, CEN (European Committee for Standardization), Brussels, Belgium, 2019.
[18] A.G. Brooks, A.K. Schindler, R.W. Barnes, Maturity method evaluated for various cementitious materials, J. Mater. Civ. Eng. 19 (12) (2007) 1017–1025.
[19] N.J. Carino, Temperature Effects on the Strength-Maturity Relation of Mortar, National Bureau of Standards, Washington, 1981.
[20] A. Mariak, M. Kurpińska, K. Wilde, Maturity curve for estimating the in-place strength of high performance concrete, MATEC Web Conf. 262 (2019) 06007.
[21] N.J. Carino, Maturity functions for concrete, in: Proceedings, RILEM International Conference on Concrete at Early Ages, Paris, I, 1982, pp. 123–128.
[22] J. Byfors, Plain Concrete at Early Ages, Technical Rep. No. 3:80, Swedish Cement and Concrete Institute, Stockholm, Sweden, 1980.
[23] EN 206+A1, Concrete: Specification, Performance, Production and Conformity, CEN (European Committee for Standardization), Brussels, Belgium, 2013.
[24] F.K. Chin, Relation between strength and maturity of concrete, ACI J. Proc. 68 (3) (1971) 196–203.
[25] J.M. Plowman, Maturity and the strength of concrete, Mag. Concr. Res. (1956,) 8.
[26] I. Galobardes, S.H. Cavalaro, C.I. Goodier, S. Austin b, Á. Rueda, Maturity method to predict the evolution of the properties of sprayed concrete, Constr. Build. Mater. 79 (2015) 357–369.
[27] A. Kuryłowicz-Cudowska, Determination of thermophysical parameters involved in the numerical model to predict the temperature field of cast-in-place concrete bridge deck, Materials 12 (19) (2019) 3089.
[28] A. Mariak, J. Chróścielewski, K. Wilde, Numerical simulation of hardening of concrete plate, Shell Struct. Theor. Appl. 4 (2018) 557–560.
[29] M. Azenha, Numerical simulation of the structural behaviour of concrete since its early ages (Ph.D. Thesis), University of Porto, 2009.
[30] G. Di Luzio, G. Cusatis, Solidification–microprestress–microplane (SMM) theory for concrete at early age: theory, validation and application, Int. J. Solids Struct. 50 (2013) 957–975.
[31] M. Cervera, R. Faria, J. Oliver, T. Prato, Numerical modelling of concrete curing, regarding hydration and temperature phenomena, Comput. Struct. 80 (2002) 1511–1521.

[32] Z.P. Bažant, W. Thonguthai, Pore pressure and drying of concrete at high temperature, J. Eng. Mech. Div. 104 (5) (1978) 1059–1079.
[33] C.E. Majorana, V. Salomoni, B.A. Schrefler, Hygrothermal and mechanical model of concrete at high temperature, Mater. Struct. 31 (6) (1998) 378–386.
[34] M. Kaszyńska, Early age properties of high-strength/high-performance concrete, Cem. Concr. Compos. 24 (2002) 253–261.
[35] J. Chróścielewski, J. Makowski, W. Pietraszkiewicz, Statyka i dynamika powłok wielopłatowych. Nieliniowa teoria i metoda elementów skończonych, 2004 (in Polish).
[36] M. Miśkiewicz, Ł. Pyrzowski, Load test of new European record holder in span length among extradosed type bridges. Seminary on geomatics, Civil and environmental engineering (2018 BGC), EDP Sci. (2018) 1–6.
[37] K.J. Bathe, Finite Element Procedures, Prentice Hall, 1982.
[38] P. Lura, K. Breugel, Thermal Properties of Concrete: Sensitivity Studies. IPACS Document, Subtask 2.5, 2001.
[39] R.H. Mills, Factors influencing cessation of hydration in water cured cement pastes, special report No. 90, in: Proceedings of the Symposium on the Structure of Portland Cement Paste and Concrete, Highway Research Board, Washington DC, USA, 1966, pp. 406–424.
[40] J. Chróścielewski, A. Mariak, A. Sabik, B. Meronk, K. Wilde, Monitoring of concrete curing in extradosed bridge supported by numerical simulation, Adv. Sci. Technol. Res. J. 10 (32) (2016) 254–262.
[41] Weather: https://www.ekologia.pl/pogoda.
[42] EN 13670, Execution of Concrete Structures, CEN (European Committee for Standardization), Brussels, Belgium, 2010.